Thoracic and Abdominal SPECT–CT Image Fusion without External Markers in Endocrine Carcinomas

Catherine Pérault, Claire Schvartz, Hubert Wampach, Jean-Claude Liehn, Marie-Joëlle Delisle and the Group of Thyroid Tumoral Pathology of Champagne–Ardenne

Nuclear Medicine and Biophysics Unit, Jean Godinot Institute, BP 171, 51056 Reims Cedex, France

Superimposition of SPECT and computed tomography (CT) slices from the thoracoabdominal region was achieved without the use of external markers for 14 studies in 13 patients with endocrine carcinoma. Technical feasibility and clinical validation of this retrospective fusion method were assessed. **Methods:** Patients had a history of thyroid cancer or of carcinoid tumor. To detect tumor sites, CT scan and dual-isotope tomoscintigraphy were performed, with ^{99m}Tc-hydroxymethylene diphosphonate for bone scintigraphy and with ^{111}In-pentetreotide, ^{131}I or ^{131}I-metaiodobenzylguanidine for tumor scintigraphy (TS). A superimposition method previously developed for the pelvic region was adapted to the nonrigid thoracoabdominal region. CT–bone scintigraphy and CT–TS superimposed images were obtained. Clinical validation of the information obtained from the superimposed images was obtained from surgery or follow-up imaging studies performed after clinical evolution of the disease process. **Results:** Reliable and reproducible registration was achieved in all patients. CT–TS superimposed images produced accurate localization of abnormal TS foci. Accuracy was limited primarily by variable relative displacements of the thoracoabdominal organs. For 10 sites in 8 patients, localization and/or characterization obtained from CT–TS images was confirmed by a reference technique. Superimposition enabled the localization of tumor sites that otherwise could not have been suspected from CT alone and allowed the characterization of CT suspicious masses and the confirmation of CT positive sites. Nonspecific tumor TS uptake sites were also localized. **Conclusion:** With standard CT and dual-isotope SPECT acquisitions, SPECT–CT fusion is feasible in the thoracoabdominal region without the use of external markers. Fused images were validated in 8 patients for 10 sites. The use of this technique could probably improve the management and care of patients with endocrine carcinoma.

Key Words: multimodality imaging; SPECT; CT; thoracoabdominal; endocrine carcinoma

J Nucl Med 1997; 38:1234–1242

Correlative image registration between functional and anatomical images has been an active research field for several years, as shown in the recent review of Weber and Ivanovic (*1*). Merging multimodality images is acknowledged to provide additional useful information for diagnosis and therapy applications. Most of the published work has been devoted to the brain, where the rigid body assumption is valid, making it possible to achieve high registration accuracy. Few multimodality image fusions have been reported in other anatomical regions such as the chest, abdomen and pelvis (*2-15*). The great majority of these registration methods use only external markers or a combination of external markers and anatomical landmarks. Few methods use exclusively internal landmarks. Among them, some are two-dimensional (*6,11*) or done with the same slice interval for the two imaging modalities (*2*); others are three-dimensional, like the method recently proposed by Yu et al. for PET and computed tomography (CT) images in the thorax (*15*) and the method that was previously developed for SPECT and CT images in the pelvic region (*9*). The purpose of this work was to extend and adapt this last method to the nonrigid thoracoabdominal region, in order to accurately localize the primary tumor or metastases in patients with endocrine carcinoma.

Several radiopharmaceuticals are known to be useful in the detection of such tumors including ^{131}I for differentiated thyroid carcinomas (DTC) and ^{131}I-metaiodobenzylguanidine (MIBG) for carcinoid tumors (CaT) (*16*). More recent radiopharmaceuticals, such as radiolabeled somatostatin analogs ^{111}In-pentetreotide (^{111}In-OctreoScan, Mallinckrodt, Petten, The Netherlands)] are being investigated for the detection of medullary thyroid carcinomas (MTC) or CaT (*17,18*). But these tumor scintigraphic (TS) images lack anatomical information. On the other hand, conventional imaging methods such as CT provide anatomical detail, but have limitations for distinguishing between malignant tissue and fibrosis, scar or inflammatory tissue and for detecting lymph node metastases or small tumors. In this context, combining TS and CT images may be of clinical utility in the management and care of the patients.

MATERIALS AND METHODS

Patients

Thirteen patients with endocrine carcinoma were selected retrospectively on the basis of abnormal TS scan result. Ten of the patients had medullary or differentiated thyroid carcinoma and had undergone total thyroidectomy. Because their serum marker level remained elevated postoperatively or because of abnormal planar TS, SPECT was performed to detect recurrence or metastases. One of the MTC patients underwent two successive studies with an interval of 8 mo in the course of the follow-up. The remaining three patients had CaT. This diagnosis was based on clinical features supported by the presence of elevated plasma serotonin level and/or urinary 5-hydroxyindoleacetic acid concentration. SPECT was performed to localize the primary tumor in two of three cases and to detect metastases in the third case. Patient characteristics are summarized in Table 1. A CT scan was performed in all patients on average 1 mo after the SPECT study. Because images were used retrospectively, no special technique was required and no additional image was obtained for this work. However, informed consent had been obtained from patients with MTC before they received ^{111}In-OctreoScan in the context of a clinical study entitled *Utility of ^{111}In-OctreoScan scintigraphy in the detection of thyrocalcitonine secreting residual MTC tissue after total thyroidectomy*, which had been approved by the regional ethical committee.

Image Acquisition

Nuclear Medicine. TS was performed using tumor-specific radiopharmaceuticals according to the different pathologies (Table 2). First, a whole-body scan and planar images, not used in this study, were obtained. Dual-isotope tumor and bone SPECT images of the neck–thoracoabdominal region were later acquired (see

Received Mar. 18, 1996; accepted Nov. 23, 1996.

For correspondence or reprints contact: Catherine Pérault, Unité de Médecine Nucléaire et de Biophysique, Institut Jean Godinot, BP 171 51056 Reims Cedex, France.

TABLE 1
Patient Characteristics

Patient No.	Primary tumor	Tumor marker: Basal (stimulated) Tg (ng/ml) normal <0.9	Basal (stimulated) TCt (pg/ml) normal <14	Plasma serotonin (μg/liter) normal: [100–300]	Urinary 5-HIAA (μmol/24 hr) normal: [26–57]
1	MTC		1500		
2	MTC		780		
3	MTC		8500		
4	MTC		1000		
5	MTC		<9 (180) in 1993		
			<9 (340) in 1994		
6	DTC	240			
7	DTC	3.7			
8	DTC	12			
9	DTC	<0.9 (<0.9)			
10	DTC	165			
11	CaT			907	
12	CaT				379
13	CaT				285

The stimulated value in parentheses is mentioned only in case of a normal basal value.
MTC = medullary thyroid carcinoma; DTC = differentiated thyroid carcinoma; CaT = carcinoid tumor; Tg = thyroglobulin; TCt = thyrocalcitonin; 5-HIAA = 5-hydroxyindoleacetic acid.

Table 2), 3 hr after the injection of 555 MBq of ^{99m}Tc-hydroxymethylene diphosphonate. The 140 keV (20% window) peak of ^{99m}Tc was used for bone scintigraphy (BS) and the two 171 keV (15% window) and 245 keV (20% window) peaks of ^{111}In or the 360 keV peak of ^{131}I (20% window) were used for TS. Patients were in the supine position with their arms extended behind their head, or if not possible, extended along their body. A large field-of-view gamma camera equipped with a parallel-hole-medium or high-energy collimator designed for ^{111}In or ^{131}I, respectively, was used. Sixty-four projections were acquired in a 64 × 64 format for 45 min through a 360° scan in the step and shoot mode.

CT. For each patient, 15–48 slices were acquired over a neck–thoracoabdominal region encompassing the observed TS abnormalities. Patients were in the supine position with their arms extended behind their head. Images were acquired during breath holding, but not always near full inspiration. The center-to-center slice spacing varied between patients and also in the same patient (range from 4–10 mm). Sometimes, slices were also acquired with different magnification factors for the same patient, when going from the upper part of the thorax down to the abdomen. Studies were discarded only if the magnification factor was such that the field of view did not contain the entire thoracic cage in the transaxial plane. Digital CT images were not available, since they were collected retrospectively and had been acquired on different systems in different radiological centers. Therefore, CT films were digitized in a 512 × 512 × 8-bit format using a CCD video camera interfaced to a personal computer by means of an acquisition card. During the digitization process, caution was taken to properly align the different images by similarly centering them in the field of view of the video camera.

Image Preprocessing

Images were sent to a Sun 4 computer for further image processing.

SPECT. BS and TS slices were reconstructed using a filtered back-projection with a Shepp–Logan filter (Hanning window). Three-dimensional smoothing was applied to low-activity TS images, i.e., ^{111}In-OctreoScan for MTC. Uniform background was then subtracted from BS and TS images with a threshold chosen so as to remove reconstruction artifacts and nonspecific activity. Hot pixel truncation was also applied to enhance low uptake areas, such as thin thoracic cage bones in BS images, which were used for the registration process. Truncation also enhanced the faint but significant TS spots.

CT. Images were reduced from a 512 × 512 format to a 256 × 256 format by pixel averaging. For each slice, the acquisition depth indicated on the film was stored in the CT header file. Slices were geometrically scaled if the magnification factor had been changed during the acquisition. Background subtraction, saturation and nonlinear gray level transformation were also applied.

TABLE 2
Tumor Scintigraphy Protocol

Tumor type	Radiopharmaceutical	Activity (MBq)	Interval between specific tracer administration and dual-isotope SPECT acquisition (days)
MTC	^{111}In-OctreoScan	220	1
DTC	^{131}I (therapeutic dose)	3700	4
CaT (2 patients)	^{111}In-OctreoScan	110	1
CaT (1 patient)	^{131}I-MIBG	37	2

MTC = medullary thyroid carcinoma; DTC = differentiated thyroid carcinoma; CaT = carcinoid tumor.

CT–TS Geometric Registration

Internal anatomical structures seen on both CT and BS, or occasionally TS, were used to determine the geometric transformation that, when applied to TS images, made them coincide with the CT images. Neither external markers nor any special acquisition technique were needed.

The Geometric Transformation. Patients were lying supine during both acquisitions, but their posture, especially arm position and neck curvature, sometimes differed between studies. Moreover, there was sometimes a variable degree of inspiration between CT slices. The difference in the respiratory dilation of the thoracic cage between the CT and SPECT images varied along the spinal axis. Indeed, the respiratory state during CT was generally near full inspiration, whereas the state during SPECT represented an average of tidal breathing. Consequently, the thoracic cage did not match between CT and SPECT images and the relative positions of abdominal organs differed between the modalities. The rigid body assumption, previously used for the pelvis, was not valid for the neck–thoracoabdominal region. A nonglobal, i.e., spatially varying, geometric transformation was then necessary to achieve a satisfactory anatomical congruence between CT and TS.

The geometric transformation was determined in a two-step process: a generally global translation and scaling along the spinal axis followed by a more or less slice-dependent translation, scaling and rotation in the transaxial plane. After the operator's recognition and selection of corresponding slices and points, the transformation parameters were automatically estimated by minimizing the sum of the squared distances between these slices and points. A linear regression or a nonlinear simplex algorithm was used for this minimization, depending on the set of parameters to be evaluated simultaneously. Technical details have been described elsewhere (*9*).

Choice of Anatomical Structures. Anatomical structures chosen as fiducials included bones, such as the spine, sternum and ribs, and soft organs below the diaphragm, such as the spleen, liver and kidneys. The choice was restricted by the limited part of the body imaged along the spinal axis. Structures were chosen in such a way that their relative orientations with respect to TS abnormal sites were approximately fixed, that is, structures were either in the neighborhood of an abnormal site or had displacements similar to this site. The anatomical correspondence was determined in a straightforward manner by pairing prominent points of these structures and also by correlating features belonging to these structures or extracted from them as described below. Centers and medial lines were used rather than uncertain edge contours.

Registration along the Spinal Axis. The parameters of the transformation along the spinal axis were estimated from the operator's selection of at least two pairs of corresponding CT and BS slices. Multiplane, i.e., frontal and sagittal in addition to transaxial slices, were used for this purpose. Prominent points such as the sternal notch and the xiphoid constituted easily identifiable markers when they were within the field of view (FOV). Useful features for the determination of homologous slices included the variation of the sternum-to-spine distance and the thoracic cage width along the spinal axis; the sternal and spinal curvatures in a sagittal plane; and the relative positions of the spleen and kidneys. Because of the relative vertical displacement between organs, different spinal axis registrations locally adapted to the organs of interest were sometimes needed. Soft organ edges were not well localized in the images and therefore organ positions along the spinal axis could not be reliably defined by identifying upper and lower boundaries. Instead of edges, organ centers, if available, and changes in size, orientation and shape along the spinal axis were identified. The resulting transformation parameters were used to build new BS and TS slices corresponding to each CT slice by linear interpolation.

Transaxial Registration. The generally slice-dependent transaxial transformation was modeled as a juxtaposition of two or three locally stationary transformations, i.e., transformations with the same parameters for a set of adjacent transaxial slices. The size of this set of slices varied for the same patient along the spinal axis and also between patients. The parameters were successively estimated for each transformation from a set of homologous point pairs selected by the operator within a set of transaxial slices that proved to share the same transformation parameters. The limits of each set of slices were moved in an iterative process until the registration quality was satisfactory. Besides well-defined fiducial points such as the centers of the sternal bone, the vertebral foramen or the kidneys, features extracted from the chest bones, e.g., the thoracic cage envelope, were used rather than the bones themselves, since it is impossible to determine exact rib-to-rib correspondence. Indeed, no simple geometric model is able to describe the dependence of relative rib displacement on the degree of inspiration and the position of the arms. Ribs were also not always easily discernible in SPECT, because their low activity could sometimes not be distinguished from the background. The thoracic cage envelope was defined for a given CT or BS transaxial slice by a smooth curve interpolated between the center of the visible ribs. Particular points on these curves were paired by the operator. These points were not chosen inside the ribs and their location was not defined with respect to the variable positions of the ribs. Rather, they were located on the curve with a precise angular position with respect to the thoracic cage axes of symmetry. For each CT slice, the parameters determined for that slice were used to build new BS and TS slices by bilinear interpolation.

Visualization of Fused Images

CT and registered SPECT slices were superimposed. The SPECT slices needed to be expanded before fusion from a 64×64 format to the 256×256 CT format. Besides the clinically relevant fused CT–TS transaxial slices, fused CT-BS slices and three-dimensional projections (*19*) were obtained. An isocontour was also drawn on BS slices to enhance the bone edges. A now classical composite color scale was used, where gray levels depicted the CT information and a geographic color scale depicted the SPECT information.

Control of the Registration Quality

Visual Assessment. The observation of the fused CT–BS slices allowed a visual qualitative assessment of the registration quality. In particular, the fused CT–BS projections assisted in verifying the registration along the spinal axis.

Accuracy of Fit. The residual root mean square (rms) error between homologous points after transaxial registration was used as an indicator of the quality of the fit.

Intra- and Interobserver Reproducibility. The initial registrations were considered the reference. Registration of the same datasets was performed several months later by the initial operator and two others. For each operator, the three-dimensional location of the TS points corresponding to a series of fixed CT points was compared to the reference TS location. The chosen CT points corresponded, according to the reference registration, to the center of all the validated abnormal high-uptake TS sites. Mean location shifts between the reference and the considered operator were compared by the nonparametric sign test. Shift variances were compared by the Fisher test. A probability of ≤ 0.05 was considered significant.

Clinical Validation

A definitive diagnosis was obtained wherever possible by surgery or by follow-up imaging studies performed after clinical evolution of the disease process. These techniques were considered as the references for the clinical validation of the superimposed images.

RESULTS

Technical Feasibility, Accuracy and Reproducibility

Reliable registration was achieved in all patients. However, the registration accuracy was different between patients because of different acquisition conditions. Among the factors influencing the ease and, hence, the reliability of the registration process were:

1. The size and location of the CT FOV along the spinal axis. Registration uncertainty along this axis was affected by whether or not well-defined fiducials fell within the FOV. Reliable fiducials included the sternal notch and xiphoid, and asymmetric features along the spinal axis such as tapering of the thoracic cage toward the apex.

2. The BS signal-to-noise ratio. The visibility of bone structures, especially the ribs, was significantly affected by the signal-to-noise ratio.

3. The magnitude of the differences in patient positioning between the CT and SPECT acquisitions. In the case of large differences between the positions of the arms and the neck or the dorsal curvatures, there were few fiducials that remained locally fixed and could thus be reliably used for calculating the geometric transformation and checking its validity, especially for the transformation along the spinal axis.

4. The magnitude of the differences in the respiratory state between CT slices and also between CT and BS. These differences not only distorted the body within the axial plane but also involved relative out-of-plane displacements of inner soft organs such as the liver, spleen, kidneys and stomach with respect to the thoracic cage.

Moreover, for a given patient, the registration accuracy was neither constant nor isotropic. Indeed, the accuracy varied with the location of the site of interest, depending on the proximity and relative mobility of this site with respect to fiducials. Deep inner structures were also assumed to be relatively less affected by the respiratory movements than external ones. Concerning the anisotropy, the accuracy was generally higher in the transaxial plane than along the spinal axis. In all cases, the accuracy was satisfactory in the transaxial plane, because within any slice or set of adjacent slices there were numerous visible structures, such as the thoracic cage, the spine or the kidneys, that allowed an unambiguous calculation and check of the transaxial registration parameters. In addition, the chosen transaxial geometric transformation model, slice-adapted translation and anisotropic scaling, was able to correctly take into account the respiratory distortion occurring to a variable extent between CT and BS. This is supported by the low rms error of 7.0 ± 1.6 mm obtained from 30 sets of about 12 points each that were selected by three different operators. On the other hand, the larger registration uncertainty along the spinal axis was essentially due to the above-mentioned limitations relating to the limited CT FOV, to the variable patient respiratory state and to differences in the patient posture between CT and TS.

From the above discussion it follows that, mainly because the acquisition conditions were not optimized and because patients undergo uncontrollable distortions, it is very difficult to obtain a meaningful numerical value as a measure of the registration accuracy. However, the above mentioned rms error of 7.0 ± 1.6 mm may be considered as a reliable estimation of the registration error in the transaxial plane for fiducials, provided they have been chosen correctly. Moreover, the intra- and interobserver registration discrepancies may also partly reflect the registration uncertainty. Three-dimensional shifts calculated from a set of 10 different CT points are given in Table 3 for 3 operators separately and all together. No significant difference was observed between the reference registration and the other three. Shift variances did not differ significantly between observers and between axes, although a trend was observed for the s.d. in the right-to-left direction (4 mm) to be smaller than in the other two directions (6–7 mm). The actual accuracy was visually assessed from the superimposed CT–BS slices and three-dimensional projections. Accuracy was found to depend on patient, site and direction and was estimated to range from less than 5 mm to about 1 cm in the transaxial plane and from 5 mm to about 2 cm along the axial axis.

TABLE 3
Intra- and Interobserver Reproducibility

Operator	x shift (mm) (mean ± s.d.)	y shift (mm) (mean ± s.d.)	z shift (mm) (mean ± s.d.)
1 (second registration) (n = 10)	1.2 ± 3.1	2.4 ± 6.7	−1.6 ± 5.8
2 (n = 10)	−1.2 ± 5.0	−0.9 ± 6.7	−1.1 ± 8.3
3 (n = 10)	−0.5 ± 4.2	−4.8 ± 7.0	1.0 ± 5.0
All (n = 30)	−0.2 ± 4.2	−1.1 ± 7.2	−0.6 ± 6.4

Reference is first registration of operator 1; x and y are, respectively, the right-to-left and top-to-bottom axes in the transaxial plane; z is the spinal axis.

Representative CT slices with the corresponding fused CT–BS and CT–TS slices are displayed in Figures 1 and 2. The superimposition images illustrate some of the points discussed above concerning the choice of fiducials used for the geometric registration and the registration accuracy.

For registration along the spinal axis, the xiphoid (Slice 8 or 9) and the manubrium at the opposite end of the sternum (Slice 2 or 7), together with the clavicles in the neighborhood of the sternoclavicular joints (Slice 5 or 6), constitute reliable fiducials, because these structures demonstrate a rapid geometric change in shape, size or position along this axis. The liver, spleen (Slice 4 or 9) and kidneys (Slice 10) offer the same advantages for local registration along this axis but are not reliable for global registration because of nonnegligible vertical displacements during breathing.

Concerning the registration within the transaxial plane, the CT and BS thoracic cage envelopes coincide well, as can be seen in almost every CT–BS image. In particular, the vertebrae and the sternum, considered as fixed fiducials, usually match well, although small rotations and shifts are sometimes observed (Slice 3 or 9). The ribs, in contrast, do not show an exact one-to-one correspondence. Moreover, ribs are not always clearly outlined in BS images; they may not be distinguishable from one another (Slice 2, 3 or 7), or they may not even be visible (Slice 9), particularly in the upper part of the thorax (Slice 5 or 6). Kidneys are also useful for the transaxial registration because they do not show any noticeable displacement within this plane during breathing (Slice 10). This is not the case for the liver and the spleen, which often show rotations and shifts and can thus be used only if they are the organs of interest. Clavicles should also be used with caution, because their spacing at a given level varies with the position of the arms (Slice 5 or 6). Scapulae cannot be used as fiducials because they

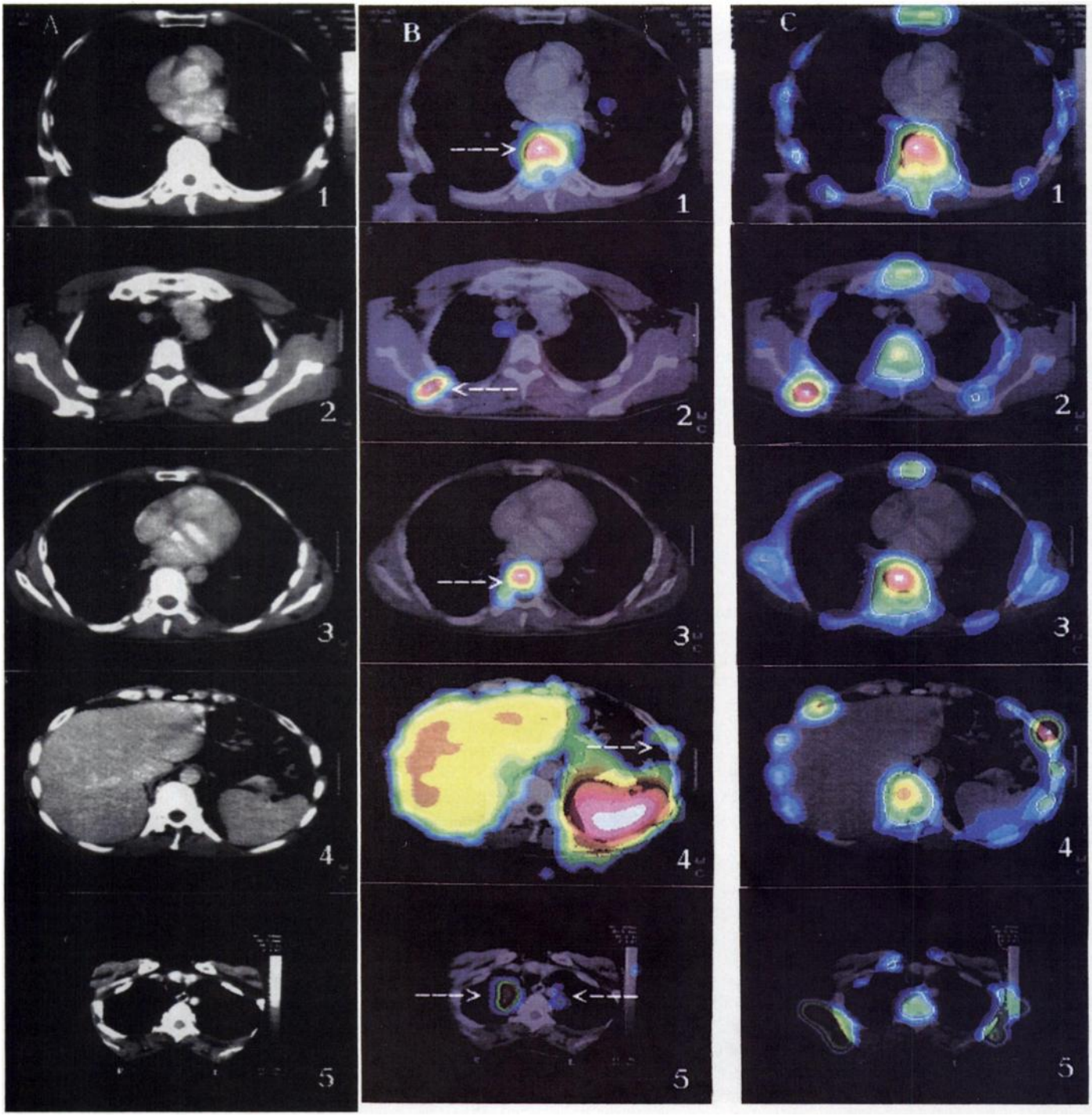

FIGURE 1. Representative slices for five validated abnormal tumor scintigraphy sites (arrows) in three patients with MTC. (A) CT alone, (B) TS–CT superimposition, (C) BS–CT superimposition. Numbers 1–5 correspond to the site numbers as described in Table 4. CT appears in gray levels, SPECT in a geographic color scale.

are sometimes out of the CT FOV (Slice 5 or 6) and often displaced with respect to the thoracic cage (Slice 3, 6 or 7).

Clinical Validation

In eight patients, the localization of pathology obtained from fused CT–TS images was validated by a reference technique for 10 abnormal high-uptake TS sites. Slices centered on these sites are shown in Figure 1 for three MTC patients and in Figure 2 for three DTC patients and two CaT patients successively. As detailed in Table 4, the histologic proof of the tissue classification of seven of these sites was obtained in one case by biopsy, and within 1 mo, by surgery in five cases and by necropsy in one case. The characterization of the three remaining sites was known from subsequent imaging, i.e., x-ray radiography, second postoperative TS and second directed CT, respectively. Three negative, two doubtful and two metastatic positive CT sites were metastases and one negative CT site proved to be the primary tumor. The two remaining negative CT sites corresponded to known nonspecific uptakes of ^{111}In-OctreoScan by inflammatory tissue and of ^{131}I by thymic residue.

DISCUSSION

We have developed a simple method for the superimposition of CT and TS slices. The time taken to digitize CT films is

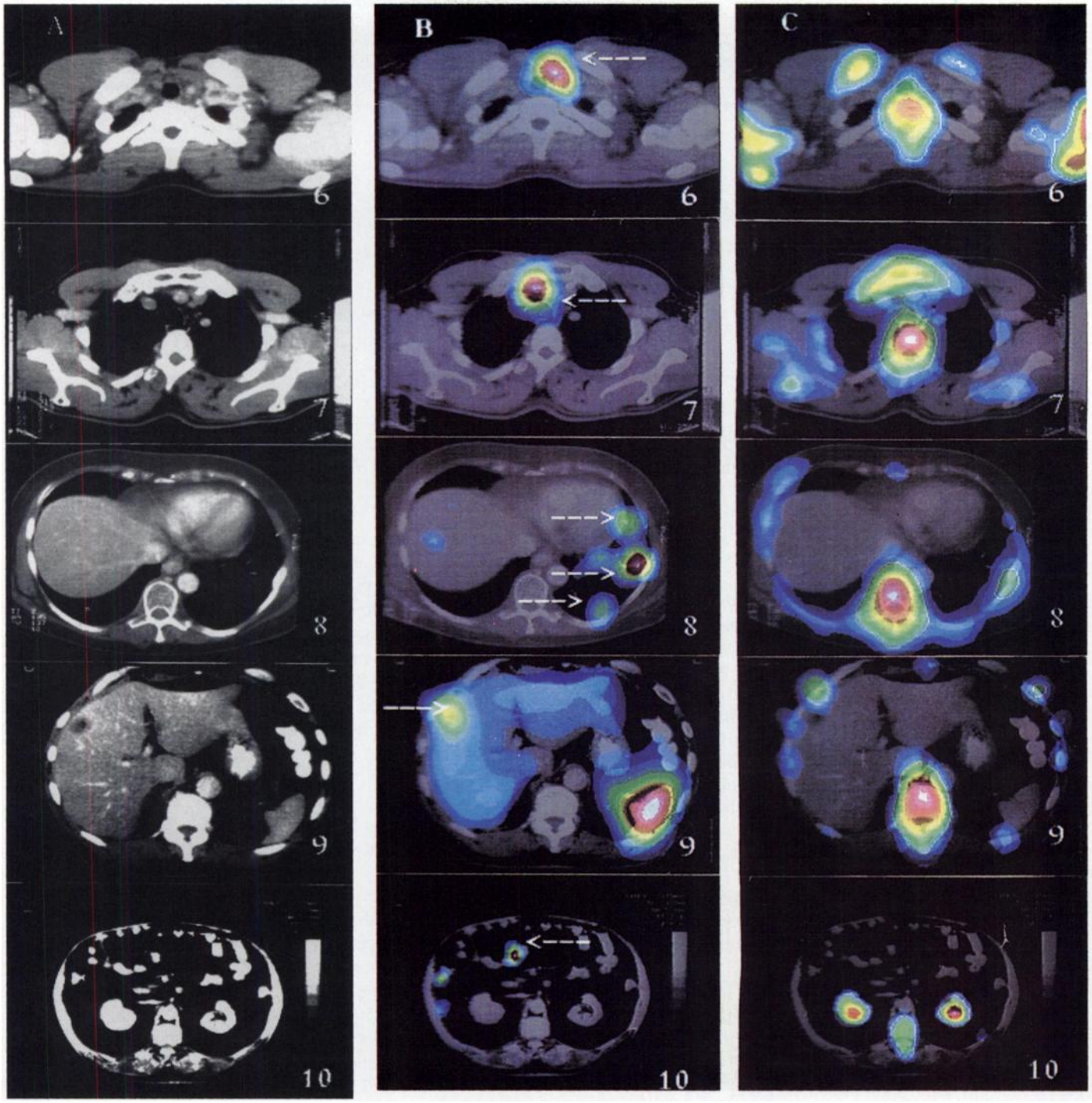

FIGURE 2. Same as in Figure 1 for the other five validated abnormal TS sites in three patients with DTC and two patients with CaT. Numbers 6–10 correspond to the site numbers as described in Table 4.

about 1 min per CT slice, once the CCD camera settings have been optimized. The total computing time is less than 2 min for 30 slices on a Sun 4 computer. The interactive part takes between 15 and 40 min, depending on the quality of the images and, to a less extent, on the experience of the operator. Some of the important and specific features of the method will now be stressed and compared to both our pelvis-adapted method and to the most similar published method developed for the thorax. Registration being the crucial part, its major characteristics will be discussed and recommendations will be given for minimizing the registration errors. Finally, the potential clinical significance will be considered.

Registration Characteristics and Limitations

Fiducials. Only internal anatomical markers were used. This offers the advantage of first allowing retrospective registrations without the requirement of any complicated acquisition protocol. Second, external markers are adequate for the head but not for the thoracoabdominal region because variable displacement of the skin relative to internal organs would adversely affect the registration errors in an uncontrollable way. The simultaneous acquisition of BS with TS is both common and useful for the localization of TS hot spots, even if no CT–TS superimposition is planned. The dual-isotope SPECT acquisition offers the advantage of a simultaneous acquisition, i.e., an exact geomet-

TABLE 4
Characteristics of Validated Abnormal Tumor Scintigraphy Sites

Patient No.	Site No.	Location	CT interpretation	Reference type	Reference diagnosis	Interval between TS and reference
1	1	Dorsal vertebra	Negative	Necropsy	Metastasis	<1 mo
2	2	Right scapula	Negative	Pain and radiography	Metastasis	2 yr
2	3	Dorsal vertebra	Metastatic	Surgery	Metastatis	<1 mo
2	4	Left rib	Metastatic	Surgery	Metastasis	<1 mo
3	5	Pleural domes	Inflammatory	Surgery	Inflammatory tissue	<1 mo
6	6	Left retroclavicular site	Negative	Surgery	Metastatic lymph nodes	<1 mo
7	7	Right retrosternal site	Negative	Surgery	Thymic residue	<1 mo
8	8	Pulmonary parenchyma	Doubtful	Postoperative TS	Metastases	7 mo
11	9	Liver	Doubtful angioma	Biopsy	Metastasis	3 mo
12	10	Small intestine	Negative	Second directed CT	Primary tumor	<1 wk

BS = bone scintigraphy; CT = computed tomography; TS = tumor scintigraphy.

ric congruence between BS and TS, which is not the case for successive transmission and emission scans used for CT–PET registration (*15*). The rib cage is very similar to the pleural surfaces of the chest wall used by Yu et al. (*15*). However, the pleural surfaces are not available in SPECT; their faintly imaged substitute, the thoracic cage, is less clearly and continuously delineated. The cage asymmetry along the spine is hidden if the top of the cage is not within the FOV. When compared with the pelvis method, prominent bone points and additional image data, such as multiplane slices, together with soft organs and features extracted from bones, e.g., thoracic cage envelope, are necessary to decrease the registration uncertainty along the spinal axis. Because of the way fiducials are chosen, the registration does not depend on the threshold chosen for the background removal. Moreover, the choice of fiducials does not require any special anatomical knowledge, because it is based only on simple comparative observations of visible features that are prominent to the untrained eye. Therefore, intra- and interobserver reproducibility proved to be satisfactory.

Registration Model. The thoracoabdominal region cannot be regarded as a nondeformable rigid object. Indeed, shape and position differences in images acquired during breath holding and during several tidal respiration cycles are not only due to different relative displacements of the diaphragm and subdiaphragmatic organs, but also to nonnegligible differences in distortion of the thoracic cage. Local transformations are then essential, at least between different transaxial slices. This was not the case for the pelvis and was not considered necessary by Yu et al., who nevertheless noticed a rostral–caudal displacement of organs in the vicinity of the diaphragm (*15*). According to our experience, distortions due to breathing should not be underestimated.

Rotations in planes different from the axial plane have been neglected, because the patient's horizontally supine position is assumed to be well aligned along the axis of the tomographic couch during both types of acquisition. This assumption is as valid for the thorax as for the pelvis.

In contrast with the method described by Yu et al., no prior knowledge of the pixel sizes was required to determine the scaling factors, which varied sometimes from slice to slice (*15*).

Registration Accuracy. Accuracy is inherently limited by the deformability of the abdominothoracic region. Registration is consequently more difficult than in the pelvic region. Relative out-of-plane movements due to respiration could not be compensated. The registration accuracy is difficult to estimate, but registration results can be checked by looking at fused CT–BS, and occasionally CT–TS, images. Three-dimensional projections were particularly useful for verifying the registration along the spinal axis, where the registration was generally difficult and the uncertainty greater than in the transverse plane.

In the fused images, a gray scale was used to depict the CT information, and a geographic scale rather than a monochrome scale was chosen to depict the SPECT information. A monochrome scale, which was chosen for the pelvis, offers the advantage of allowing better visibility of the CT information. On the other hand, a geographic scale makes it easier to check the adequacy of the registration, because it provides several isocontours simultaneously from which the centering of a scintigraphic structure on a CT structure can be assessed. Moreover, the visibility of faint BS or TS structures is enhanced with a geographic scale because regions of low count density are not displayed at low intensities.

The rms error in the transaxial plane was less than the SPECT pixel size of 8.45 mm. This finding probably results from a consistent choice of fiducials, an adequate geometric transformation model and the ability for the algorithm to minimize the image matching criterion. However, this does not ensure a "correct" match, because the chosen fiducials might not be truly corresponding points. No rms error was reported along the spinal axis, because too few pairs of homologous slices could generally be selected for this value to be meaningful.

The intra- and interobserver registration discrepancies were also less than the SPECT pixel size and resolution.

Goodness of fit and reproducibility are partial indicators of the registration accuracy, but the major contribution to the registration error remains unknown, because recognition of truly corresponding slices and points is sometimes challenging and because points of interest do not always follow the same geometric transformation as fiducials. A numerical or physical phantom with well-defined markers and a simple known geometric transformation between both acquisitions would not answer this question. It would only give an optimal error value (*20*). Even a very sophisticated phantom with relative displacements between different parts would only give an error for a specific configuration, which could not be related to a given patient. The important thing to know for each patient is what uncertainty is attached to the localization on CT images of a given high-uptake TS site. This can only be obtained by a careful observation of the superimposition images.

Acquisition Recommendations for Minimizing the Registration Errors

Based on our experience with the registration difficulties discussed above, the following simple acquisition requirements should be fulfilled in order to minimize the registration errors.

CT and SPECT. The patient position should be as similar as possible between both acquisitions. In particular, the positions of the arms, head and neck should be the same. Because of conflicting arguments, the choice of the preferable position for the arms remains an unsolved problem. Indeed, arms extended behind the head is the usual position during CT scans and probably provides a higher image quality for CT and SPECT. But this position is less comfortable and, compared with arms extended along the body, induces more patient movement during SPECT acquisition.

CT. A constant degree of inspiration should be maintained from slice to slice. If possible, a mid-inspiration state should be chosen to closely resemble the mean tidal state characteristic of SPECT. Spiral CT, where about 30 slices are acquired during one held breath, promises to eliminate variations between CT slices related to the state of inspiration.

If digital data were available and slices were acquired with the same magnification factor and centering, the residual image alignment uncertainty occurring during the digitization procedure would be eliminated. Moreover, digital data would shorten the manual processing and would avoid the degradation of CT image quality.

The FOV should contain the whole thoracic cage within the transaxial plane. Also, it should not be too small along the spinal axis and should contain the upper part of the thoracic cage as well as the sternal notch and xiphoid for thoracic imaging.

SPECT. To optimize the bone scintigraphy quality, the acquisition duration should be as long as possible and a sufficient activity should be injected. However, the ^{99m}Tc-hydroxymethylene diphosphonate activity should be limited to minimize dual-isotope ^{111}In-^{99m}Tc artifacts (*21*). Indeed, ^{111}In windows are contaminated by "ghost" photons arising from the summation of two accidentally coincident ^{99m}Tc photons. Because of its much higher photopeak energy, ^{131}I should not be affected by this artifact. In Figure 1, the vertebra uptake (Slices 1 and 3), scapula uptake (Slice 2) and very faint rib uptake (Slice 4) are not due to these artifacts. The count ratio between ^{111}In and ^{99m}Tc, calculated over the suspect region, is too high to be ascribed completely to contamination for the vertebrae and scapula. The absence of exact geometric coincidence between the ^{99m}Tc and ^{111}In spots also excludes the possibility of a contamination artifact for the rib. However, we observed a TS high uptake in the shoulder, not shown here, which was very probably artifactual based on the ratio between ^{111}In and ^{99m}Tc counts.

Potential Clinical Role

Our purpose was first to assess the feasibility and validity of a CT–SPECT fusion method by retrospective use of patient images in various parts of the thoracoabdominal region and in different clinical contexts. We think it important, however, to analyze the potential clinical impact of these fused images. In spite of the registration accuracy limitations, the CT–TS superimposition images, when compared with separate CT and TS images, help establish the anatomical correspondence between CT and TS localizations, i.e., between morphological and physiological forms of information. The geometric accuracy of this correspondence, or at least the confidence in conclusions drawn from standard clinical practice for image comparison, is increased by image fusion. In some cases, an exact anatomical correspondence cannot be determined, but one can affirm that a TS spot does or does not belong to a given organ. This restricted knowledge may be sufficient for the diagnosis. Fused images are more useful but also less accurate for soft tissues, e.g., pulmonary parenchyma (Sites 5 and 8), lymph nodes, liver (Site 9) and intestine (Site 10), than for bones (Sites 1–4) or sites near bones, e.g., retroclavicular (Site 6) and retrosternal (Site 7). Indeed, in the latter case, the information is directly known from BS or deductible from the simple comparison of both sets of images.

Let us now consider the diagnostic implications of a more accurate or reliable localization of CT and TS sites with respect to one another. The meaning of an enhanced TS uptake depends on its precise localization. If it corresponds to a positive (Sites 3–5) or doubtful (Sites 8 and 9) CT site, the pathological nature of the tissue is confirmed. If, in contrast, it corresponds to a negative CT site, two cases should be considered. First, if the site is known to show nonspecific uptake, e.g., stomach or thymic residue for ^{131}I (Site 7), it is considered normal, which eliminates a false-positive TS interpretation. Second, in the opposite case (Sites 1, 2, 6 and 10), an infraradiological site may be discovered and precisely located.

Beyond the diagnostic utility, these fused images may influence the patient management and care by guiding the choice of biopsy sites, by avoiding a useless biopsy (Site 9) or by providing surgeons with valuable information for surgical decision and planning refinement (Sites 5–8).

CONCLUSION

We have developed a simple noninvasive retrospective technique for registering and superimposing CT and SPECT images in the thoracoabdominal region. This was demonstrated to be feasible without the use of external markers and with standard CT and dual-isotope SPECT acquisitions. The technique was applied to 14 studies in patients with endocrine carcinoma and validated for 10 sites in eight patients. It probably increases the diagnostic power of each separate imaging modality for the detection and localization of recurrence or metastases.

ACKNOWLEDGMENTS

The SPECT images with ^{111}In-OctreoScan were acquired in the context of a study entitled: *Utility of ^{111}In-OctreoScan scintigraphy in the detection of thyrocalcitonine secreting residual MTC tissue after total thyroidectomy*, sponsored by Mallinckrodt Medical B.V. (Petten, The Netherlands). We thank our colleagues in the medical and technical team of the Nuclear Medicine and Biophysics Unit who participated in patient management and image acquisition. We also thank Catherine Mead for revising the original English version and especially Prof. E. Chaney (University of North Carolina, Chapel Hill, NC) for his contributions to the final version of the manuscript.

REFERENCES

1. Weber DA, Ivanovic M. Correlative image registration. *Semin Nucl Med* 1994;24: 311–323.
2. Pitcher EM, Stevens PH, Davies ER, Goddard PR, Jackson PC. Transfer and combination of digital image data. *Br J Radiol* 1985;58:701–703.
3. Lumbroso JD. Digital superimposition of single photon emission computerized tomography (SPET) and CT images for immunoscintigraphy. In: Srivastava SC, ed. *Proceedings of the NATO advanced study institute: radiolabeled monoclonal antibodies for imaging and therapy*. New York: Plenum Press; 1986:541–550.
4. Kaplan IL, Swayne LC. Composite SPECT–CT images: technique and potential applications in chest and abdominal imaging. *Am J Roentgenol* 1989;152:865–866.
5. Kramer EL, Noz ME, Sanger JJ, Megibow AJ, Maguire GQ. CT–SPECT fusion to correlate radiolabeled monoclonal antibody uptake with abdominal CT findings. *Radiology* 1989;172:861–865.
6. Birnbaum BA, Noz ME, Chapnick J, et al. Hepatic hemangiomas: diagnosis with fusion of MR, CT and Tc-99m-labeled red blood cell SPECT images. *Radiology* 1991;181:469–474.

7. Kramer EL, Noz ME. CT-SPECT fusion for analysis of radiolabeled antibodies: applications in gastrointestinal and lung carcinoma. *Nucl Med Biol* 1991;18:27–42.
8. Maguire GQ, Noz ME, Rusinek H, et al. Graphics applied to medical image registration. *IEEE Comput Graph Appl* 1991;2:20–27.
9. Liehn JC, Loboguerrero A, Pérault C, Demange L. Superimposition of computed tomography and single photon emission tomography immunoscintigraphic images in the pelvis: validation in patients with colorectal or ovarian carcinoma recurrence. *Eur J Nucl Med* 1992;19:186–194.
10. Loats H. CT and SPECT image registration and fusion for spatial localization of metastatic processes using radiolabeled monoclonals. *J Nucl Med* 1993;34:562–566.
11. Sgouros G, Chiu S, Pentlow KS, et al. Three-dimensional dosimetry for radioimmunotherapy treatment planning. *J Nucl Med* 1993;34:1595–1601.
12. Wahl RL, Quint LE, Cieslak RD, Aisen AM, Koeppe RA, Meyer CR. "Anatometabolic" tumor imaging: fusion of FDG PET with CT or MRI to localize foci of increased activity. *J Nucl Med* 1993;34:1190–1197.
13. Kato T, Fukatsu H, Ito K, et al. Fluorodeoxyglucose positron emission tomography in pancreatic cancer: an unsolved problem. *Eur J Nucl Med* 1995;22:32–39.
14. Scott AM, Macapinlac H, Zhang J, et al. Image registration of SPECT and CT images using an external fiduciary band and three-dimensional surface fitting in metastatic thyroid cancer. *J Nucl Med* 1995;36:100–103.
15. Yu JN, Fahey FH, Gage HD, et al. Intermodality, retrospective image registration in the thorax. *J Nucl Med* 1995;36:2333–2338.
16. Hanson MW, Feldman JM, Blinder RA, Moore JO, Coleman RE. Carcinoid tumors: iodine-131 MIBG scintigraphy. *Radiology* 1989;172:699–703.
17. Reubi JC, Modigliani E, Calmettes C, Kvols L, Krenning EP, Lamberts SWJ. In vitro and in vivo identification of somatostatin receptors in medullary thyroid carcinomas, pheochromocytomas and paragangliomas. In: Calmettes C and Guliana JM, eds. *Proceedings of the "Colloque INSERM": medullary thyroid carcinoma*. Montrouge, France: John Libbey Eurotext Ltd; 1991;211:85–87.
18. Krenning EP, Kwekkeboom DJ, Bakker WH, et al. Somatostatin receptor scintigraphy with [^{111}In-DTPA-D-Phe^1]- and [^{123}I-Tyr^3]-octreotide: the Rotterdam experience with more than 1000 patients. *Eur J Nucl Med* 1993;20:716–731.
19. Loboguerrero A, Pérault C, Liehn JC. Volume rendering and bicolor scale in double isotope studies: application to immunoscintigraphy and bone landmarking. *Eur J Nucl Med* 1992;19:201–204.
20. Scott AM, Macapinlac HA, Divgi CR, et al. Clinical validation of SPECT and CT/MRI image registration in radiolabeled monoclonal antibody studies of colorectal carcinoma. *J Nucl Med* 1994;35:1976–1984.
21. Miles KA, Barber RW. A man with three knees? false "hot spot" with dual isotope imaging. *Br J Radiol* 1990;63:798–800.

(continued from page 9A)

FIRST IMPRESSIONS
Triple Ventricle Sign

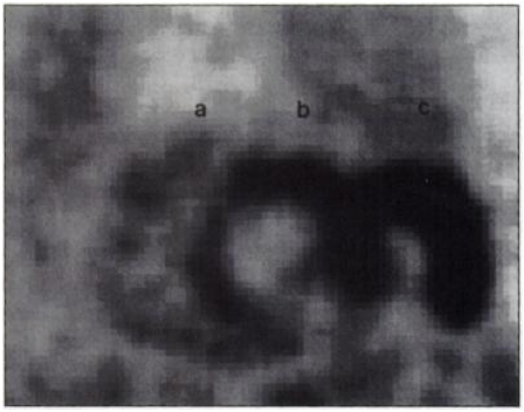

Figure 1.

Figure 2.

Purpose
A 58-yr-old man with a history of inferior wall myocardial infarction was evaluated following angina during coronary angiography. Reversible ischemia was suspected, so the patient was referred for stress-rest myocardial perfusion imaging using ^{99m}Tc-tetrofosmin. Unexpectedly, the rest images demonstrated uptake in three semicircular structures (Fig. 1). Chest radiograph showed elevation of the diaphragm and pericardiac air in the bowel (Fig. 2, arrow). In addition to uptake in the right and left ventricle, the scintigraphic findings of a third ventricle were caused by physiologic excretion of activity from the liver into the bowel (Fig. 1).

Tracer
Technetium-99m-tetrofosmin, 500 MBq

Route of Administration
Intravenous

Time after Injection
Rest images, 1 hour

Instrumentation
Toshiba GCA-9300/HG triple-head gamma camera

Contributors
Marcel Stokkel, Berthe van Eck-Smit and Koos Blokland, Department of Diagnostic Radiology and Nuclear Medicine, University Hospital Leiden, The Netherlands.